

ANALYSIS AND SIMPLIFIED DESIGN OF PRECAST JOINTED DUCTILE CONNECTIONS

A. Palermo¹, S. Pampanin²

¹Assistant Professor, Dept. of Structural Engineering, Politecnico di Milano, Piazza Leonardo da Vinci 32, 20133, Milan, Italy, email: palermo@stru.polimi.it;

²Senior Lecturer, Dept. of Civil and Natural Resources Engineering, University of Canterbury, Christchurch, New Zealand, email: stefano.pampanin@canterbury.ac.nz.

ABSTRACT :

This paper describes simplified design tools for precast concrete hybrid system/connections developed during the PRESSS (PREcast Seismic Structural Systems) project, where unbonded post-tensioned tendons/bars are adequately combined with longitudinal mild steel or supplemental damping devices. In order to design the hybrid connections, which are subjected to a controlled rocking motion under an earthquake excitation, a section analysis procedure to evaluate the moment-rotation behaviour of the connection has been proposed in literature by the authors, and validated through a series of experimental tests. In this contribution, a parametric analysis on different section profiles is carried out in order to investigate the principal parameters affecting the moment-rotation capacity of hybrid sections. Either structural parameters, i.e. unbonded length of cables/tendons, mild steel, element length and section parameters, i.e. mechanical ratios of unbonded cables/tendons, mild steel, axial ratio have been considered in the parametric studies. On the basis of these results design charts to be used within a simplified design procedure have been developed. Furthermore an approximate closed-form solution for rectangular sections with lumped mild steel reinforcement has been derived and proposed. The two section analysis approaches are then implemented and compared within a worked example of a hybrid structural connection, designed according to a direct displacement-based approach.

KEYWORDS: Precast concrete, hybrid connections, unbonded post-tensioning, design charts.

1. INTRODUCTION

Recent developments in the research of precast/prestressed concrete structures for seismic areas following the pioneering work carried out under the PRESSS project, coordinated by the University of California, San Diego [Stanton et al., 1997], [Priestley et al. 1999] have resulted in the experimental validation of different innovative typologies of ductile connections for moment resisting frames and wall systems. A particularly efficient and flexible solution was offered by the hybrid system where unbonded post-tensioned tendons/bars with self-centring properties are adequately combined with longitudinal mild steel or supplemental damping devices, which can provide appreciable energy dissipation. The inelastic demand is lumped at the critical section (beam-to-column, wall or column-to-foundation) through opening and closing of an existing gap at the interface. A sort of “controlled rocking” motion of the beam or wall/column occurs, while the relative ratio of post-tensioning and mild steel governs the hysteretic “flag-shaped” cyclic behaviour, typical of these systems. A uniquely high seismic performance is achieved since the damage of the connection is limited to the “yielding” of the mild steel reinforcement or alternative dissipation devices (based on friction and/or viscous mechanisms) which act as fuses or shock absorbers during the rocking motion, preserving the integrity of the main structural elements. Experimental and numerical investigations are still ongoing to refine this new-generation of seismic resisting systems based on PRESSS-technology, while several on site applications have already been implemented in different seismic-prone countries around the world, including U.S., Europe, South America, Japan, and New Zealand [Pampanin, 2005]. Code design provisions are currently available in an extensive form in the New Zealand Concrete Standard [[NZS3101:2006, Appendix B]; in other documents [fib, 2004], [ACI 550R-96, ACI 550.1R-01, 2001] design guidelines and analytical section-analysis procedure to predict moment capacity (vs. gap opening) of hybrid connections have been illustrated.

The aim of this paper is to provide further simplified tools to accurately predict the moment-rotation capacity of

hybrid connection at critical performance levels. Based on the section analysis moment-rotation procedure proposed by [Pampanin et al., 2001], adopted in the fib [2004] and in the [NZS3101:2006] and subsequently refined by [Palermo, 2004], an extensive parametric analysis has been carried out for different section profiles (square, rectangular, hollow-rectangular and circular), and reinforcement layout for beams, columns, walls and piers systems, with different mechanical and geometrical properties. As a main outcome, design charts as well as closed-form solutions are derived and herein proposed for a quick while reliable hand-calculation design of hybrid connection.

2. SECTIONAL ANALYSIS APPROACH

In a controlled rocking system, an infinite curvature is developed at the critical section due to the opening and closing of a single “crack” (gap) at the interface. Therefore, a moment-rotation relationship shall be adopted over a traditional moment-curvature relationship when defining the section behavior. Also due to the presence of unbonded post-tensioned tendons and of a partially unbonded length in the mild steel, section strain compatibility between the concrete and steel is violated at the critical interface (Fig. 1). This requires the introduction of an alternative compatibility condition at a global (member) level, as suggested by the Monolithic Beam Analogy, MBA, [Pampanin et al. 2001; fib, 2004; Palermo, 2004; NZS3101:2006, Appendix B]. According to this procedure, a member compatibility condition is provided by imposing equal member deflections between a system implementing a hybrid connection and an equivalently reinforced concrete (monolithic) solution. As a result, internal material strains, stresses, forces and moment contributions (from the mild steel reinforcement, post-tensioned tendons and axial load) can be evaluated relating to the peculiar gap opening mechanism. Figure 1 shows the gap opening and closing mechanism as well as the distribution and evaluation of material strain in a generic pier section subjected to bending moment M , axial load N and post-tensioning T_{pt} . For a given rotation, θ , the depth of the neutral axis, c , corresponds to a unique solution respecting both the equilibrium equations at a section level and compatibility conditions at a member level. A complete moment vs. rotation response can thus be derived.

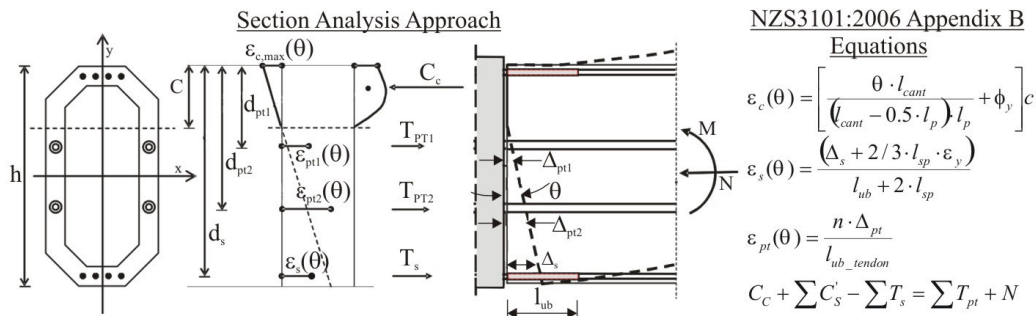


Figure 1 - Section analysis approach for a hybrid connection and equations proposed in the Concrete Standard NZS3101:2006, Appendix B.

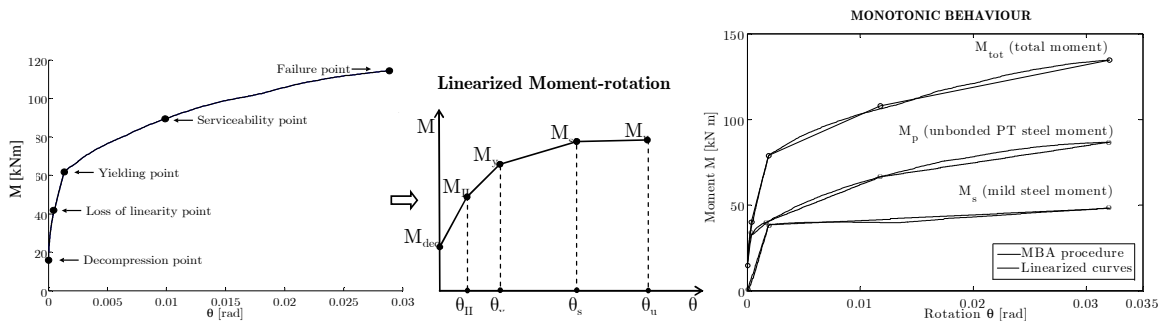


Figure 2 – a) Fundamental points of a typical moment-rotation relationship; b) linearized curves and self-centering vs, dissipative contributions

Figure 2 shows the resultant moment-rotation relationship and its linearization corresponding to the following

fundamental performance levels: 1) the decompression point, where, in correspondence of moment M_{dec} , the gap θ starts to open; 2) the loss of linearity point, briefly named point II (θ_{II} , M_{II}), as proposed by [Priestley & Tao, 1983], [El-Sheikh et al., 1997] corresponding to the occurrence of a sudden change of stiffness due to geometric non-linearity following the relocation of the neutral axis depth. This typically occurs at a moment $M_{II} \cong 2-2.5 M_{dec}$; if $M_{II} \geq M_y$ the point II is assumed equivalent to the yielding point; 3) the yielding point (θ_y , M_y), corresponding to either the yielding of the mild steel ($\varepsilon_s = \varepsilon_{sy}$) or the achievement of a concrete strain $\varepsilon_c = 0.002$, whichever occurs first; 4) the serviceability point (θ_s , M_s), corresponding to the crushing of the cover concrete ($\varepsilon_c = 0.004$, with spalling assumed to occur at $\varepsilon_c = 0.0064$) or the achievement of a mild steel strain $\varepsilon_s = 0.01$ whichever occurs first; 5) the failure point (θ_u , M_u), corresponding to the occurrence of ultimate strain in one of the two materials: concrete strain $\varepsilon_c \cong 0.02$ or $\varepsilon_s = 0.06$ [Priestley & Kowalsky, 1998] suggested these definitions of M_y , M_s , M_u for a linearized moment-curvature behavior for reinforced concrete sections. The aim of the following analyses is to similarly extend the evaluation of hybrid connections behaviour for design or analysis purposes, by evaluating the basic points of a linearized moment-rotation behavior corresponding to specific levels of performance.

3. PARAMETRIC ANALYSIS

The moment-rotation procedure proposed in [Palermo, 2004], developed from the previous procedure proposed by [Pampanin et al., 2001] has been implemented into a software program PAPADI [Palermo et al. 2004]. Extensive parametric analyses of hybrid connections considering different section profiles and reinforcement layout have been carried out and used to develop design charts. A summary of the results is given herein; more details can be found in [Palermo, 2004]. Figure 3 shows the geometrical data of the different section profiles considered in the parametric analysis, i.e. square, hollow-rectangular, wall-rectangular and circular sections. Lumped reinforcement at the top and bottom of the section and distributed reinforcement, as represented in Figure 3, have been investigated. A confined concrete model [Mander et al., 1988] was adopted, while for the mild steel reinforcement and the post-tensioned cables/tendons the hysteretic model proposed by [Dodd & Restrepo-Posada, 1995] was implemented.

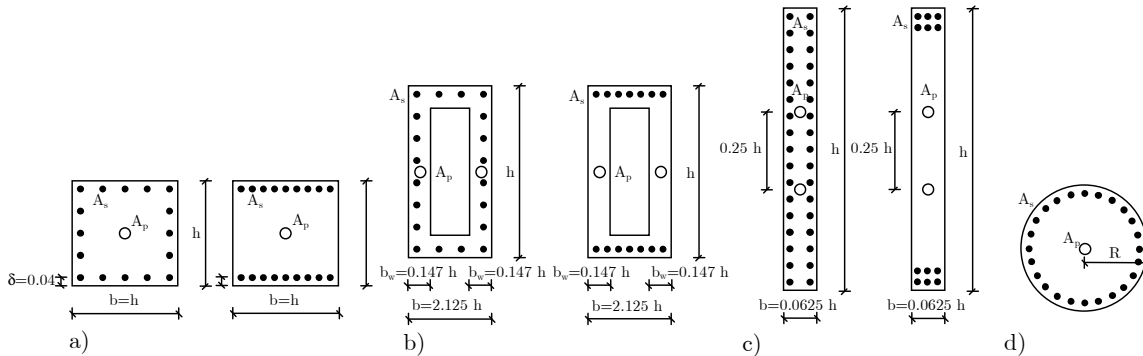


Figure 3. Different section profiles analyzed with distributed and lumped mild steel reinforcement:
 a) square section; b) rectangular-hollow section; c) wall-rectangular section; d) circular sections

Contrary to reinforced concrete sections, the moment-rotation (gap opening) curves of an unbonded post-tensioned dissipative connection (hybrid) is affected by several additional structural parameters, as the column element height or beam cantilever length L (distance from the point of contraflexure to the rocking section where gap opening occurs), the unbonded length of the cable/tendon L_{pub} , the unbonded length of mild steel L_{sub} . Figure 4 shows, for the case of square section with lumped reinforcement, the moment-rotation curves obtained by varying the unbonded length of the tendons (L_{pub}/L) and the mild steel reinforcement (L_{sub}/L), respectively. As expected, for both cases the moment capacity at the serviceability level is not changed; the loss of linearity point, briefly named point II (θ_{II} , M_{II}), is instead drastically reduced when (L_{pub}/L) increases. At the ultimate limit state (or failure) level, since the rupture of mild steel reinforcement may govern the hybrid

section failure, an increasing of (L_{sub}/L) would correspond to high values of maximum gap opening (Figure 4). However, in the design process, when a level of rotation $\theta = 0.02$ (drift $\approx 2\%$) is typically considered, the variation of the two above-mentioned unbonded length parameters, L_{upb} and L_{sub} , does not significantly affect the response in terms of moment-rotation (opening of the gap). Regarding the section parameters, the mechanical ratios of unbonded cable/tendon, $\omega_p = f_{py}A_p/f_{co}'hb$ and mild steel reinforcement, $\omega_s = f_{sy}A_s/f_{co}'hb$ have been varied within a range 0.02 to 0.3 (with increment of 0.02). In addition, the axial load ratio ν is varied within the range of $0 \leq \nu \leq 0.6$. The initial stress f_{p0} of unbonded cables/tendons is fixed to $0.6 f_{pu}$. Dimensionless moment-axial load interaction diagrams ($\nu = N/f_{co}'hb$, $\mu = M/f_{co}'h^2b$), are derived for different level of ω_s for assigned values of ω_p .

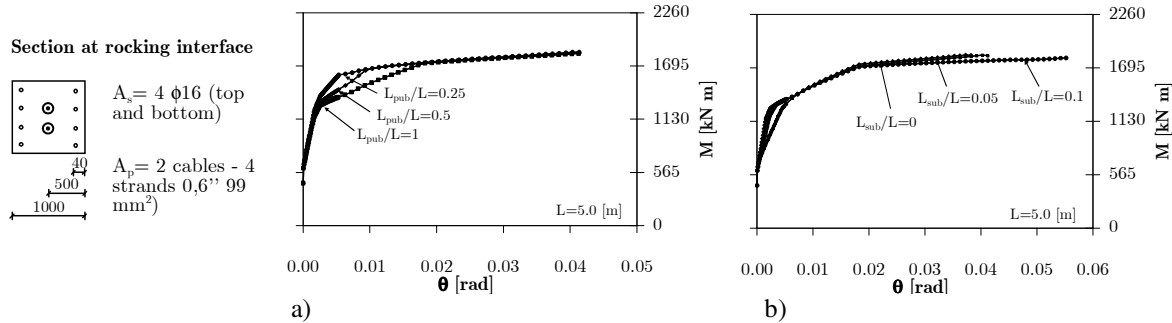


Figure 4 - Moment vs. rotation (gap opening) varying L_{pub}/L and L_{sub}/L .

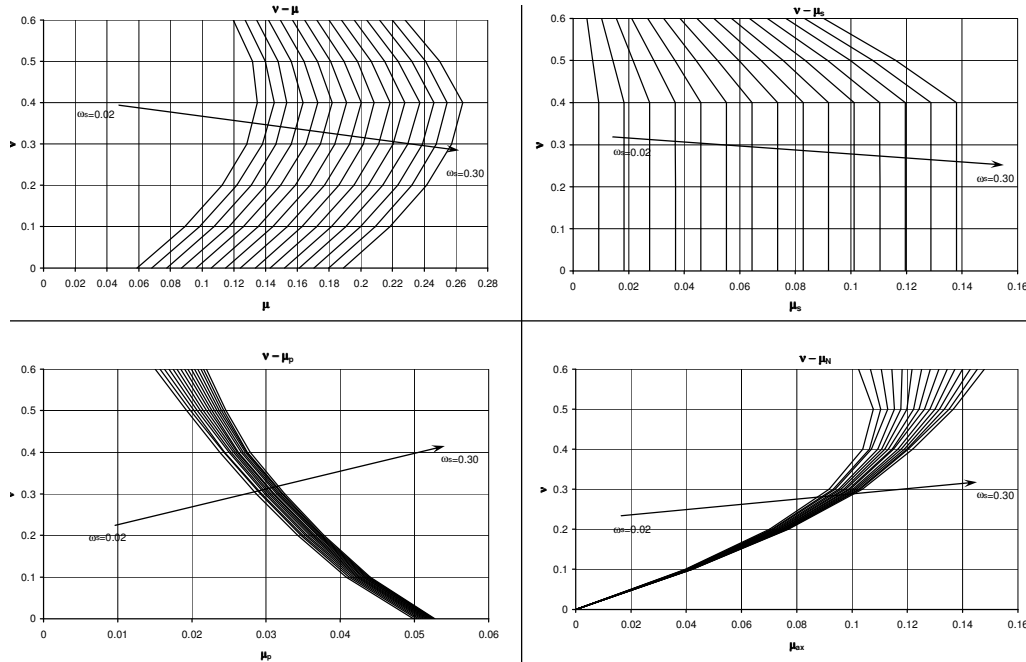


Figure 5. ν vs. μ at serviceability level ($\omega_p=0.14$; $\omega_s=0.02$; 0.04; ... ; 0.28; 0.30)

Figure 5 shows the contribution in terms of ν - μ diagrams of the mild steel reinforcement, of the unbonded post-tensioned cables and the axial load, for the specific case of a square section with lumped mild steel reinforcement. Increasing ω_s , i.e. mild steel reinforcement, the total section moment capacity is incremented. The axial load ratio ν strongly reduces the moment capacity of the section for values greater than 0.4. For each design level (yielding, serviceability and ultimate), more detailed information are given through related tables (Table 1), where the dimensionless neutral axis position ξ (c/d), the gap opening θ , the dimensionless stresses for the mild steel reinforcement α_{sc} (top - compression) and α_{st} (bottom - tension), for the unbonded post-tensioned tendon α_p and for the concrete (maximum compressive stress) α_c are reported.

Table 1 – section parameters at yielding, serviceability and ultimate level ($\omega_p=0.14$; $\omega_s=0.08$)

ν	μ_{yield}	$\mu_{yield,(s)}$	$\mu_{yield,(p)}$	$\mu_{yield,(N)}$	θ_{yield}	ξ_{yield}	$\alpha_{yield,(st)}$	$\alpha_{yield,(sc)}$	$\alpha_{yield,(p)}$	$\alpha_{yield,(c)}$
0.0	0.0732	0.0353	0.0388	0.0000	0.0084	0.3	-0.997	0.418	-0.691	0.710
0.1	0.1056	0.0355	0.0353	0.0371	0.0091	0.4	-1.000	0.637	-0.681	0.914
0.2	0.1295	0.0335	0.0319	0.0681	0.0092	0.5	-0.921	0.833	-0.670	1.028
0.3	0.1313	0.0215	0.0270	0.0883	0.0061	0.6	-0.527	0.849	-0.656	1.028
0.4	0.1272	0.0146	0.0223	0.0977	0.0038	0.7	-0.256	0.861	-0.652	1.028
0.5	0.1150	0.0110	0.0175	0.0956	0.0020	0.9	-0.064	0.869	-0.654	1.028
0.6	0.0935	0.0095	0.0125	0.0810	0.0004	1.1	0.080	0.875	-0.663	1.028

ν	μ_{serv}	$\mu_{serv,(s)}$	$\mu_{serv,(p)}$	$\mu_{serv,(N)}$	θ_{serv}	ξ_{serv}	$\alpha_{serv,(st)}$	$\alpha_{serv,(sc)}$	$\alpha_{serv,(p)}$	$\alpha_{serv,(c)}$
0.0	0.0870	0.0368	0.0509	0.0000	0.0290	0.1	-1.000	1.000	-0.824	1.137
0.1	0.1167	0.0368	0.0418	0.0403	0.0196	0.3	-1.000	1.000	-0.741	1.138
0.2	0.1402	0.0368	0.0353	0.0721	0.0151	0.4	-1.000	1.000	-0.699	1.137
0.3	0.1562	0.0368	0.0299	0.0952	0.0123	0.5	-1.000	1.000	-0.671	1.141
0.4	0.1636	0.0368	0.0250	0.1092	0.0104	0.6	-1.000	1.000	-0.653	1.143
0.5	0.1560	0.0291	0.0207	0.1153	0.0089	0.7	-0.720	1.000	-0.641	1.136
0.6	0.1418	0.0211	0.0169	0.1145	0.0076	0.8	-0.398	1.000	-0.633	1.136

ν	μ_{ult}	$\mu_{ult,(s)}$	$\mu_{ult,(p)}$	$\mu_{ult,(N)}$	θ_{ult}	ξ_{ult}	$\alpha_{ult,(st)}$	$\alpha_{ult,(sc)}$	$\alpha_{ult,(p)}$	$\alpha_{ult,(c)}$
0.0	0.0907	0.0368	0.0559	0.0000	0.0637	0.2	-1.000	1.000	-0.977	0.713
0.1	0.1116	0.0368	0.0420	0.0365	0.0444	0.3	-1.000	1.000	-0.822	0.715
0.2	0.1267	0.0368	0.0324	0.0632	0.0333	0.4	-1.000	1.000	-0.731	0.721
0.3	0.1316	0.0368	0.0246	0.0782	0.0272	0.5	-1.000	1.000	-0.673	0.708
0.4	0.1278	0.0368	0.0184	0.0827	0.0222	0.6	-1.000	1.000	-0.636	0.716
0.5	0.1123	0.0368	0.0128	0.0751	0.0188	0.7	-1.000	1.000	-0.608	0.716
0.6	0.0813	0.0368	0.0071	0.0523	0.0166	0.8	-1.000	1.000	-0.585	0.698

4. SIMPLIFIED DESIGN METHODS

The results of the parametric analyses carried out in Paragraph 3 becomes a powerful tool for design purposes; the design of hybrid sections can be implemented by using above mentioned $N-M$ or dimensionless $\nu-\mu$ interaction diagrams/design charts, as typically done for traditional reinforced concrete sections. In addition to a design approach based on design charts, approximate close form solution can be adopted, as described in paragraph 4.2 (at this stage limited, for simplicity, to square/rectangular columns and walls with lumped mild steel reinforcement at the top and bottom of the section profile).

4.1. $\nu-\mu$ design charts approach

The design procedure is based on the use of three main parameters, namely the design bending moment and axial load and the targeted self-centering condition governed by the λ parameter, i.e. ratio between the re-centering moment contribution, $M_{pr} + M_N$, provided by the post-tensioning and the axial load, and the dissipative moment contribution, M_s , provided by the mild steel or other dissipaters. Typically, it is recommended that λ be bigger than 1.25, in order to guarantee a full re-centering condition, and preferably no greater than 2.0-3.0, to optimize the energy dissipation capacity of the system (Eq. 4.1).

$$\lambda = \frac{M_p + M_N}{M_s} \geq 1.25 \quad (4.1)$$

Since $M = M_p + M_N + M_s$, the relationship between the moment contribution (or dimensionless moment $\mu = M/f_{co}bh^2$) and the re-centering condition λ can be written as:

$$M_s = \frac{M}{1+\lambda}; \quad \mu_s = \frac{M_s}{f_{co}bh^2}; \quad M_p + M_N = \frac{M\lambda}{1+\lambda}; \quad \mu_p + \mu_N = \frac{M_p + M_N}{f_{co}bh^2} \quad (4.2)$$

Once the self-centering and dissipation dimensionless moment capacities as well as the axial ratio ν are known, the required mechanical reinforcement ratios for both mild steel and post-tensioned steel ω_s and ω_p can be easily found using the above mentioned interaction diagram and design charts ($\mu_s - \nu$, $\mu_p - \nu$, $\mu_N - \nu$) shown in Fig. 5 and Table 1. At a first step, a serviceability level limit state can be assumed during the design process. The actual gap opening θ is then checked to be consistent within the targeted structural performance (e.g. 2% of drift). Interpolation between the serviceability (or ultimate) and the yielding points provided by the charts might be required. From the mechanical steel ratios ω_s , ω_p , the actual internal mild steel (A_s , A_s') and unbonded post-tensioned tendons (A_p) can then be derived, after assuming the element section dimensions.

4.2. Approximate section-equilibrium approach

An approximate section-equilibrium solution based on concrete stress block assumptions at ultimate conditions is herein briefly presented for rectangular sections with lumped mild steel reinforcement. When compared to the simplified design provisions provided by the [ACI, 2001] proposal, some additional parameters are accounted for as the influence of the re-centering condition parameter λ and the contribution of the axial load ratio ν . Three conditions are imposed: the translational equilibrium, the rotation equilibrium about the centroid of the concrete compressive force and a self-centering condition (Figure 6). The compatibility equations for the materials are the same ones reported in Figure 1. About α and β are the concrete stress block coefficients as proposed by [Popovics, 1970], $K = f_{cc}'/f_{co}'$ is the confinement effect ratio between the maximum confined concrete compressive stress f_{cc}' and the unconfined concrete compressive stress f_{co}' .

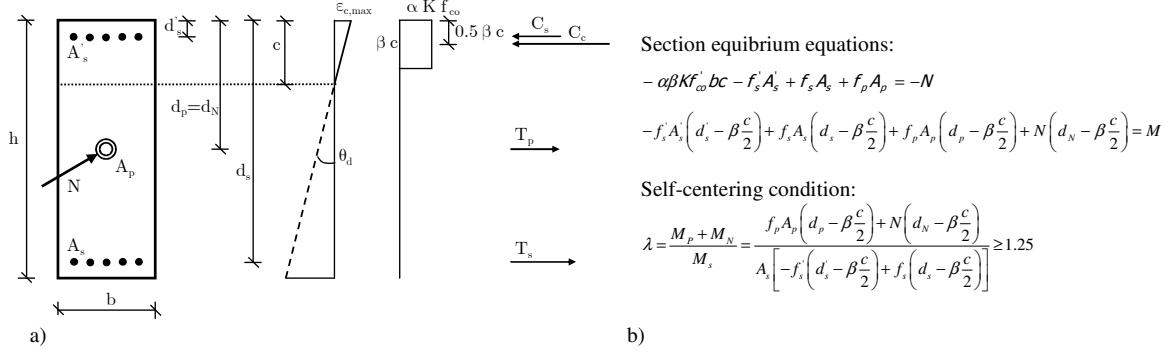


Figure 6. a) Section analysis details; b) equilibrium equations and self-centering condition

By assuming the same amount of mild steel reinforcement at top and bottom of section, i.e. $A_s = A_s'$ and dividing the two section equilibrium equations by $f_{co}'hb$, $f_{co}'h^2b$, respectively, the following dimensionless formula can be obtained

$$-\alpha\beta K\xi + (-\alpha_s' + \alpha_s)\omega_s + \alpha_p\omega_p = \nu \quad (4.3)$$

$$\omega_s \left[-\alpha_s' \left(\delta_s' - \beta \frac{\xi}{2} \right) + \alpha_s \left(\delta_s - \beta \frac{\xi}{2} \right) \right] + \alpha_p \omega_p \left(\delta_p - \beta \frac{\xi}{2} \right) + \nu \left(\delta_N - \beta \frac{\xi}{2} \right) = \mu \quad (4.4)$$

$$\lambda = \frac{f_p A_p \left(d_p - \beta \frac{c}{2} \right) + N \left(d_N - \beta \frac{c}{2} \right)}{A_s \left[f_s \left(d_s - \beta \frac{c}{2} \right) - f_s' \left(d_s' - \beta \frac{c}{2} \right) \right]} \quad (4.5)$$

where $\xi = c/h$ is the dimensionless neutral axis position, α_s , α_s' , α_p , δ_s' , δ_s , δ_p , are the dimensionless stresses and distances (from the top of section) of mild steel, unbonded cable/tendon, respectively and δ_N is the dimensionless distance of the axial load from the top of the section. The above mentioned parametric analyses confirmed that $\alpha_s \approx \alpha_s'$, thus from Eq. (4.6) the dimensionless neutral axis ξ can be simplified as:

$$\xi \cong \frac{1}{\alpha\beta K} (\nu + \alpha_p \omega_p) \quad (4.6)$$

By substituting $\delta_p = \delta_p' = 1/2$ in Eqs. (4.4), (4.5) and inserting Eq. (4.6) in Eq. (4.4) a second order equation, the dimensionless neutral axis position ξ can be obtained within the solution shown in Eq. (4.7). For an assigned target rotation θ_d , the material strains and thus non-dimensional material stresses α_s , α_s' , α_p , can be easily evaluated from the section mechanism shown in Fig. 1 and according to the procedure reported in [Palermo, 2004]. Finally, mechanical ratios ω_s , ω_p can be respectively expressed as reported in Eq. 4.7.

$$\xi \cong \frac{1}{2\beta} \cdot \left(1 \pm \sqrt{1 - \frac{8\mu\lambda}{\alpha K(1+\lambda)}} \right); \quad \omega_s \cong \frac{\mu}{\alpha_s(1+\lambda)(\delta_s - \delta_s')}; \quad \omega_p \cong \frac{1}{\alpha_p} \left(\frac{\lambda\mu}{0.5(1+\lambda)(1-\beta\xi)} - \nu \right) \quad (4.7)$$

In order to assess the validity of the design solution and confirm the above mentioned simplified hypotheses the following checking must be carried out (see Eq. 4.8). In particular, the first checking is necessary in order to obtain real positive values for the neutral axis position ξ ; the assumed hypothesis $\alpha_s \approx \alpha_s'$, is granted only if the

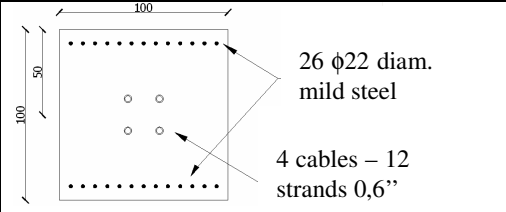
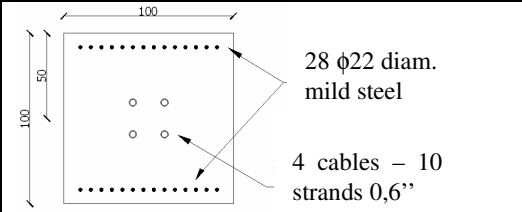
second checking is satisfied, while the third one is referred to control that the increase in stress Δf_p in the unbonded cable due to the opening of the gap would maintain the tendons in the elastic domain.

$$\frac{8\mu\lambda}{\alpha K(1+\lambda)} \leq 1; \quad 100 \cdot \frac{(\alpha_s - \alpha'_s)\omega_s}{\alpha_p \omega_p + \nu} \leq 10-15\%; \quad \Delta f_p = E_p \cdot \frac{n\theta_d h \left(\frac{1}{2} - \xi\right)}{L_{pub}} \leq (f_{py} - f_{p0}) \quad (4.8)$$

5. WORKED EXAMPLE

A single degree of freedom hybrid-rocking bridge pier prototype (1000 x 1000 mm section, 8 meter high), has been designed according to a Direct Displacement Based Design Approach [Priestley et al., 2007] for a design drift level of 2%, resulting into a required moment $M = 5000$ kNm. Since the dimensionless axial ratio ν value was lower than 0.05, for simplicity, during the design process the axial load contribution has been in this instance neglected. A lumped distribution of mild steel reinforcement (fully bonded along the length, i.e. $L_{sub} = 0$) is adopted, while the unbonded length for the post-tensioned tendons is assumed to correspond to the pier height, i.e. $L_{sub} / L = 1$.

Table 2 – Section data and design results for section equilibrium and design charts approach

parameter	value	parameter	value	parameter	value	parameter	value
ν	0	f_{co}'	45 MPa	λ	1,5	δ'_s	0,04
β	0,7	f_p	1130 MPa	α_s	1	δ_s	0,96
$K=f_{cc}'/f_{co}'$	0,7	f_c'	430 MPa	α'_s	1	δ'_p	0,5
$B=h$	1000 mm	f_s'	430 MPa	α_p	0,6976	δ_N	0,5
f_{cc}'	52 MPa	μ	0,111				
Approximate section-equilibrium approach				Design chart approach			
ω_s	0.096	ξ	0.295	ω_s	0.10	ξ	0.25
ω_p	0.241	λ	1.7	ω_p	0.22	λ	1.54
							

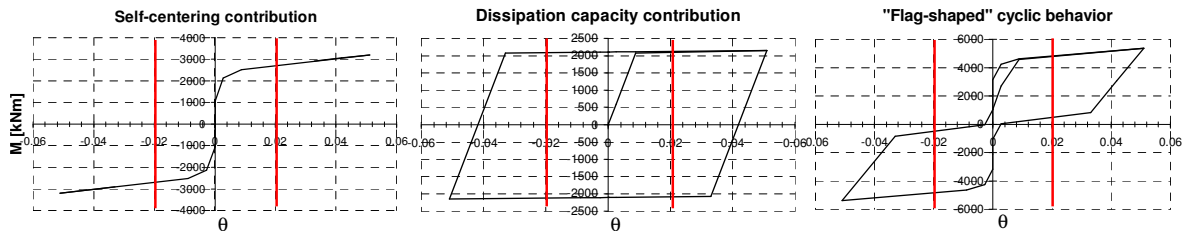


Figure 7. Design chart solution: moment vs. rotation contributions

The design λ parameter has been assumed equal to 1.5. The other mechanical and geometrical parameters are reported in the upper part of Table 2. The two above mentioned simplified design approaches (design charts or simplified closed-form solution) have been applied to this case and compared following the design steps reported in paragraph 4.1 and 4.2. As reported in the lower part of table 2, the design chart method allows to obtain a more precise design in terms of self-centering condition (actual 1.54 vs. targeted 1.5 with design chart; actual 1.7 vs. targeted 1.5 with the closed-form solution). However, the differences in terms of mild reinforcement between the two approaches are negligible (less than 7%), while due to the higher value of λ obtained during the design process for section-equilibrium approach an increment of 12% respect to design charts approach is observed. The final hybrid section layout is shown in the lower part of Table 2. A full validation of the design results, herein not reported, has been successively carried out with PAPADI program. Once the section reinforcement has been designed, the moment capacity at the above mentioned design levels for each single contribution (axial load, unbonded tendons, internal mild steel reinforcement) can be calculated.

Linearizing the moment moment-rotation curves and assuming an Elasto-plastic cyclic behaviour for the mild steel reinforcement and a Non-Linear elastic cyclic behaviour for the self-centering contribution (axial load + unbonded tendons) the typical flag-shaped cyclic behaviour can be obtain as results of the sum of these two contribution, as shown in Figure 7 (design charts method). The vertical red lines refer to the target gap-opening corresponding to the target 2% drift. The equivalent viscous damping, $\xi_{equiv}=5+100(1-\mu_{\Delta}^{-1})/(\pi(1+\lambda))$, measuring the energy dissipated by the system (μ_{Δ} =drift ductility), is almost equal to 18% at the target drift.

6. CONCLUSIONS

In this paper, two simplified design approaches for unbonded post-tensioned hybrid connections are proposed, based on either design M-N interaction diagrams or on a closed-form solution for section analysis, and validated through an focus-oriented section-analyses program for hybrid connections. The parametric analyses carried out allowed to develop design charts for a variety of section profiles and reinforcement layout, while the section equilibrium-approach presented is at this stage limited to rectangular sections only. Both methods are satisfactorily reliable, the design chart method being more accurate, the close-form section equilibrium probably being more intuitive and simple to implement. More extensive parametric analyses on additional section profiles, considering different dissipation devices are ongoing with the intent to provide further support and confidence to practitioner engineers for the design and analysis of these emerging seismic resisting systems.

REFERENCES

- ACI Committee. "Design Recommendations for Precast Concrete Structures". (ACI 550R-96) (Reapproved 2001); "Emulating Cast-in-Place Detailing in Precast Concrete Structures". (ACI 550.1R-01), 2001.
- Dodd, L. L., Restrepo-Posada J. I., (1995). Model for Predicting Cyclic Behavior of Reinforcing Steel, *Journal of Structural Engineering*, ASCE, Vol. 121, No. 3, pp. 433-445.
- El-Sheikh M, Pessiki S, Sause R, Lu L-W, Kurama Y., (1997). Seismic Analysis, Behavior, and Design of Unbonded Post-tensioned Precast Concrete Frames; Earthquake Research Report, Report No. EQ-97-02, Department of Civil and Environmental Engineering, Lehigh University, Bethlehem, PA, November.
- fib, International Federation for Structural Concrete, (2004). Seismic Design of Precast Concrete Building Structures, Bulletin 27, Lausanne, 254 pp.
- NZS 3101:2006. Standards New Zealand, Design of Concrete Structures, Appendix B: Special Provisions for the Seismic Design of Ductile Jointed Precast Concrete Structural Systems.
- Mander, J. B., Priestley, M. J. N., Park, R. (1988). Theoretical Stress-strain Model for Confined Concrete, *Journal of Structural Engineering*, Vol. 114, No. 8, pp. 1804-1826.
- Palermo A., S. Pampanin, D. Bolognini (2004). PAPANI. Moment-rotation Procedure FORTRAN-Program for Hybrid Concrete Elements, Department of Structural Engineering, Politecnico di Milano, Italy.
- Palermo, A. (2004). The Use of Controlled Rocking in the Seismic Design of Bridges, Ph.D. thesis, Department of Structural Engineering, Politecnico di Milano, Italy.
- Pampanin, S., Priestley, M. J. N., Sritharan, S. (2001). Analytical Modelling of the Seismic Behaviour of Precast Concrete Frames Designed with Ductile Connections, *Journal of Earth. Eng.*, 5(3), 329-367.
- Pampanin S., (2005). Emerging Solutions for High Seismic Performance of Precast/Prestressed Concrete Buildings", *Journal of Advanced Concrete Technology (ACT)*, invited paper for Special Issue on "High performance systems", Vol. 3 (2), pp. 202-22
- Popovics S. (1970). A Review of Stress-Strain Relationships for Concrete, *ACI Journal*, Vol. 67, No. 3, pp. 243-248.
- Priestley, M. J. N., Tao J. (1993). Seismic Response of Precast Prestressed Concrete Frames with Partially Debonded Tendons. *PCI Journal*, Vol. 38, No. 1, pp. 58-69.
- Priestley M J N, Kowalski M J., (1998). Aspects of Drift and Ductility Capacity of Cantilever Structural Walls, *Bulletin, New Zealand Society for Earthquake Engineering*, Vol. 31, No. 2, June.
- Priestley, M. J. N., Sritharan, S., Conley, J. R., Pampanin, S. (1999). Preliminary Results and Conclusions From the PRESSS Five-Story Precast Concrete test Building, *PCI Journal*, Vol. 44, No. 6, pp. 42-67.
- Priestley, M.J.N., Calvi, G.M. and Kowalsky, M.J. (2007). Displacement-based seismic design of structures. IUSS Press, Pavia, Italy.
- Stanton, J. F., Stone, W. C., Cheok, G. S. (1997). A Hybrid Reinforced Precast Frame for Seismic Regions, *PCI Journal*, Vol. 42, No. 2, pp. 20-32.